Data-Aided Timing Synchronization for FM-DCSK UWB Communication Systems

Shaoyuan Chen, *Student Member, IEEE*, Lin Wang, *Senior Member, IEEE*, and Guanrong Chen, *Fellow, IEEE*

***Abstract*—Frequency-modulated differential chaos shift keying (FM-DCSK) ultrawideband (UWB) communication systems convey information by transmitting ultrashort chaotic pulses (in the nanosecond scale). Since such pulses are ultrashort, timing offset may severely degrade the bit error rate (BER) performance. In this paper, a fast data-aided timing synchronization algorithm with low complexity is proposed for FM-DCSK UWB systems, which capitalizes on the excellent correlation characteristic of chaotic signals. Simulation results show that the BER performance of such systems is fairly close to that of perfect timing thanks to the proposed new algorithm. Moreover, the new algorithm requires less synchronization searching time and lower computational complexity than the conventional one for transmitted reference UWB systems existing in the current literature.**

***Index Terms*—Frequency-modulated differential chaos shift keying (FM-DCSK), timing synchronization, transmitted reference (TR), ultrawideband (UWB).**

I. Introduction

ULTRAWIDEBAND (UWB) communication technology attracts increasing interest for its promising potential in many applications with low-complexity and low-power requirements, particularly in short-range wireless communications such as wireless personal area networks (WPANs) and sensor networks [1].

UWB impulse radio systems convey information by transmitting ultrashort (in the nanosecond scale) pulses. The monocycle pulses could have Gaussian, Rayleigh, or other shapes [2]. In order to collect the rich multipath energy in the dense multipath environment, the UWB system based on coherent detection exploits a Rake receiver with many fingers, but what must be done prior to that is channel estimation. Unfortunately, channel estimation requires high sampling rates at several gigahertz and complicated processing techniques [3], [4]. Alternatively, a noncoherent transmitted reference (TR) UWB system, as proposed in [5], tries to capture the entire signal energy without requiring channel estimation. Frequency-modulated differential chaos shift keying (FM-DCSK) [6] UWB [7] system offers another type of noncoherent TR UWB scheme, which uses nonperiodic chaotic signal as the carrier [8], [9]. As an outstanding joint spread-spectrum and modulation scheme, FM-DCSK is proven to have a superior capability of antimultipath fading over multipath fading channels [10]–[13].

Since UWB information-bearing pulses are ultrashort, timing offset may remarkably deteriorate the bit error rate (BER) performance [14], [15]. Hence, timing synchronization is a major challenge for the implementation of UWB receivers. Currently, there are very few, if any, studies on the timing synchronization issue in the literature about the FM-DCSK UWB system. Nevertheless, there are several papers (e.g., [3] and [16]–[18]) that deal with the timing synchronization problem for coherent UWB by correlating the template signal with the received signal to meet the timing acquisition. However, since FM-DCSK UWB is noncoherent, timing synchronization algorithms applied to noncoherent UWB have to be developed. The existing algorithms derived in [19] and [20] for noncoherent TR UWB both rely on the following two operations: 1) the operation of correlation between two neighboring symbols and 2) the operation of picking the peak from a large amount of correlation values. However, the former operation is not available for the FM-DCSK UWB system for the following two reasons: 1) a chaotic waveform varies from symbol to symbol, even if the same bit is transmitted repeatedly [7], which is the main difference between the FM-DCSK UWB and the conventional noncoherent TR UWB, and 2) noise-like chaotic signals have low values of intersymbol correlation. Consequently, the peak-picking operation cannot be carried out correctly in general.

In this paper, a new data-aided timing synchronization algorithm with rapidity and low complexity is proposed for the FM-DCSK UWB communication system. The algorithm is based on intrasymbol correlation operation, which takes advantage of the excellent correlation characteristic of chaotic signals. Through extensive simulations, it is found that not only the BER performance of the synchronized system equipped with the proposed timing algorithm is close to that of perfect timing, but also the synchronization can be rapidly achieved. Moreover, the algorithm has fairly low computational complexity.

The remainder of this paper is organized as follows. Section II introduces the system model. Section III describes the new timing synchronization algorithm, and Section IV presents the simulation results. Finally, conclusion is drawn in Section V.

II. System Model

The FM-DCSK UWB system model is similar to the fixed-waveform TR UWB system architecture, as illustrated in Fig. 1, where the main difference is the waveform generator. Moreover, the FM-DCSK has an extra frequency modulator.

Manuscript received January 1, 2009; revised December 1, 2009. First published December 31, 2009; current version published April 14, 2010. This work was supported in part by the City University of Hong Kong under Strategic Research Grant 7002453, in part by the National Natural Science Foundation of China under Grant 60972053, and in part by the Natural Science Foundation of Fujian Province under Grant 2008J0035.

S. Chen and L. Wang are with the Department of Communication Engineering, Xiamen University, Fujian 361005, China (e-mail: wanglin@xmu.edu.cn).

G. Chen is with the Department of Electronic Engineering, City University of Hong Kong, Kowloon, Hong Kong.

Digital Object Identifier 10.1109/TIE.2009.2038402

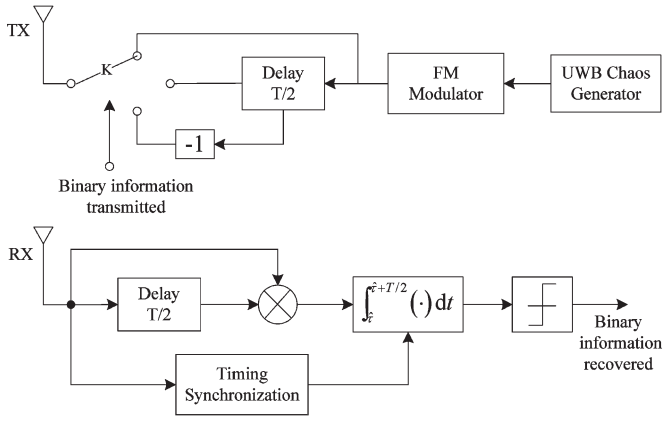

Fig. 1. Block diagrams of the FM-DCSK UWB transmitter (TX) and receiver (RX).

In this system, each symbol contains only one frame. Each frame consists of two parts: the first part serves as a reference signal, whereas the second part serves as the data signal, which is either a replica of the reference when the transmitted bit is "+1" or an inverted signal when the bit is "−1."

The FM-DCSK UWB signal can be represented as

$$s(t) = \sum_{k=-\infty}^{\infty} \left[p^{(k)}(t - kT) + d_k p^{(k)}(t - kT - T/2) \right]. \quad (1)$$

Here, k is the symbol index, T is the symbol period, $d_k \in \{\pm 1\}$ is the transmitted bit, $p(t)$ is the frequency-modulated chaotic pulse of width T_w, and $p^{(k)}(t)$ indicates that $p(t)$ varies from symbol to symbol. In this paper, it is assumed that $T_w \ll T/2$, so neither intersymbol interference nor interpulse interference exists in the system.

The channel model of UWB can be described as a tapped delay line [21] as follows:

$$h(t) = \sum_{l=0}^{L-1} \alpha_l \delta(t - \tau_l). \quad (2)$$

Here, L is the total number of resolvable multipath taps, and α_l and τ_l are the complex amplitude gain and the delay of the lth tap, respectively, with $\tau_0 < \tau_1 < \cdots < \tau_{L-1}$, where τ_0 is the propagation delay of the first arrival signal. Assume that the channel is quasi-static, which means that $h(t)$ remains invariant over every one symbol period of time.

The received waveform passing through the channel filter, which is not shown in Fig. 1 for simplicity, is given by

$$\begin{aligned} r(t) &= s(t) \otimes h(t) + n(t) \\ &= \sum_{l=0}^{L-1} \alpha_l s(t - \tau_l) + n(t) \\ &= \sum_{k=-\infty}^{\infty} \left[\sum_{l=0}^{L-1} \alpha_l p^{(k)}(t - kT - \tau_l) \right. \\ &\qquad \left. + d_k \sum_{l=0}^{L-1} \alpha_l p^{(k)}(t - kT - T/2 - \tau_l) \right] + n(t). \end{aligned} \quad (3)$$

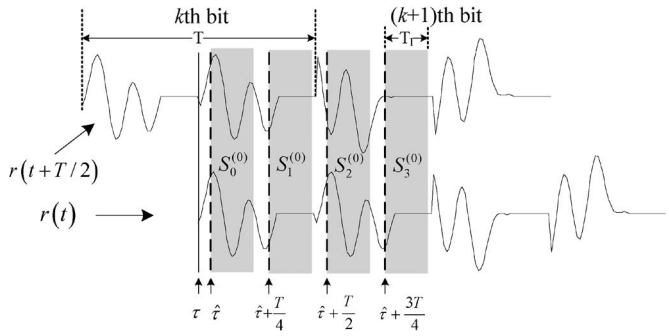

Fig. 2. Timing algorithm at step 0 ($N = 4$).

Here, $\otimes$ is the convolution operation, and $n(t)$ is the zero-mean additive complex Gaussian noise with variance N_0.

In order to demodulate the data and recover the original information correctly, the receiver must have information about the symbol boundary, i.e., the integral starting point, which is tied to the timing synchronization.

III. Timing Algorithm

In this section, a new data-aided synchronization algorithm is presented for estimating the ideal integral starting point.

A. Algorithm

Let τ denote the ideal integral starting point. At the very beginning, the receiver does not know the exact arrival time of the incoming signal. Thus, the ideal integral starting point is unknown by the receiver. Assume that the receiver arbitrarily locates the integral starting point to be at $nT + \hat{\tau}$, where n is an integer. Without loss of generality, one may set $n = 0$ and $\hat{\tau} \in [\tau, \tau + T)$, as partially illustrated in Fig. 2, where noise is neglected for simplicity. Theoretically, the objective of the timing synchronization is equivalent to achieving

$$\hat{\tau} \in [\tau - T_{\rm res}, \tau + T_{\rm res}]. \quad (4)$$

Here, $T_{\rm res}$ is the synchronization resolution (see Section IV).

The algorithm is being performed in the following steps.

Step 0: Divide the interval $[\hat{\tau}, \hat{\tau} + T]$ into N parts uniformly and take the beginning point of each part as the integral starting point. Thus, within one symbol observation interval, N integral results are obtained, i.e.,

$$S_i^{(0)} = \left| \int_{\hat{\tau}+iT/N}^{\hat{\tau}+iT/N+T_I} r(t) \times r^*(t + T/2) dt \right|, \quad i = 0, 1, \ldots, N-1. \quad (5)$$

Here, $*$ is the conjugation operator, $|(\cdot)|$ is the magnitude of $(\cdot)$, and $T_I \in [T_w, T/2]$ is the integral window length in the timing synchronization stage. In Section IV, it will be shown that different values of T_I can result in different timing performances.

Define

$$I = \arg\max_i S_i^{(0)}, \qquad i = 0, 1, \ldots, N-1. \quad (6)$$

Then, the receiver can update $\hat{\tau}$ according to

$$\hat{\tau} = \hat{\tau} - \mathrm{mod}\left((N-I)T/N, T\right). \tag{7}$$

Here, $\mathrm{mod}(a,b)$ gets the remainder of a/b.

In the above, (5)–(7) can be explained as follows. Suppose that $N=4$ and the additive Gaussian noise is not considered. Using (5), one obtains four integral results $S_0^{(0)}$, $S_1^{(0)}$, $S_2^{(0)}$, and $S_3^{(0)}$, but which one is the largest depends on the location of the initial integral starting point $\hat{\tau}$. Take the position of $\hat{\tau}$ in Fig. 2 for example. As $\hat{\tau}$ is quite near τ, $S_0^{(0)}$ is the largest in the receiver because $S_0^{(0)}$ captures more useful signal energy than both $S_1^{(0)}$ and $S_3^{(0)}$. The reason $S_0^{(0)} > S_2^{(0)}$ is that the correlation between the chaotic waveforms for two different symbols is very small, which is a promising feature of chaotic signals. Thus, from (6), one has $I=0$. Substituting $I=0$ into (7) yields $\hat{\tau} = \hat{\tau}$, which means that $\hat{\tau}$ need not be updated after this step since $\hat{\tau}$ is quite near τ. Notice that the discussion here is based on the assumption of $\hat{\tau}$ being quite near τ. Although $\hat{\tau}$ is initially uniformly distributed in $[\tau, \tau+T)$, (5)–(7) work well.

After step 0, the target interval, in which τ lies, can be determined in $[\hat{\tau}-T/N, \hat{\tau}+T/N]$ whose length is $2T/N$.

Step q: For $q \geq 1$, perform the following: Through step $q-1$, it is known that τ lies in the interval $[\hat{\tau}-T/(2^{q-1}N), \hat{\tau}+T/(2^{q-1}N)]$, which is then uniformly divided into two subintervals, namely, $[\hat{\tau}-T/(2^{q-1}N), \hat{\tau}]$ and $[\hat{\tau}, \hat{\tau}+T/(2^{q-1}N)]$. The purpose of this step is to determine in which subinterval τ lies, and the determination is based on (8)–(11) given as follows:

$$S_j^{(q)} = \left| \int_{\hat{\tau}-(-1)^j \frac{T}{2^q N}}^{\hat{\tau}-(-1)^j \frac{T}{2^q N}+T_I} r(t) \times r^*(t+T/2)dt \right|, \qquad j=0,1. \tag{8}$$

Equation (8) indicates two integral operations whose integral starting points, namely, $\hat{\tau}-T/(2^qN)$ and $\hat{\tau}+T/(2^qN)$, are the middle points of the above two candidate subintervals, respectively.

If $S_0^{(q)} > S_1^{(q)}$, then it can be verified that τ lies in $[\hat{\tau}-T/(2^{q-1}N), \hat{\tau}]$ because $S_0^{(q)}$ collects more useful signal energy than $S_1^{(q)}$ when τ lies in $[\hat{\tau}-T/(2^{q-1}N), \hat{\tau}]$; otherwise, $\tau \in [\hat{\tau}, \hat{\tau}+T/(2^{q-1}N)]$ according to the following equation:

$$\tau \in \begin{cases} \left[\hat{\tau}-\frac{T}{2^{q-1}N}, \hat{\tau}\right], & \text{if } J=0 \\ \left[\hat{\tau}, \hat{\tau}+\frac{T}{2^{q-1}N}\right], & \text{if } J=1. \end{cases} \tag{9}$$

Here

$$J = \arg\max_j S_j^{(q)}, \qquad j=0,1. \tag{10}$$

Hereafter, the receiver locates $\hat{\tau}$ in the middle point of the interval determined by (9) to keep $\hat{\tau}$ as close to τ as possible, i.e.,

$$\hat{\tau} = \begin{cases} \hat{\tau}-\frac{T}{2^qN}, & \text{if } J=0 \\ \hat{\tau}+\frac{T}{2^qN}, & \text{if } J=1. \end{cases} \tag{11}$$

Thus, the length of the target interval in which τ lies is shortened to be $T/(2^{q-1}N)$, and the maximum timing error is half of the target interval length, i.e., $T/(2^qN)$, according to (9) and (11). Then, update $q=q+1$. If $q > q_{\mathrm{prop}}$, the algorithm ends; otherwise, repeat step q. Here, q_{prop} is defined in (13).

The least number of steps that the proposed algorithm needs to achieve the timing synchronization depends on the synchronization resolution T_{res}. It is clear that the number of steps is sufficient if (12) is satisfied, which means that the maximum timing error is less than or equal to the resolution, i.e.,

$$\frac{T}{2^qN} \leq T_{\mathrm{res}}. \tag{12}$$

Thus, one has

$$q \geq \log_2 \frac{T}{NT_{\mathrm{res}}}. \tag{13}$$

Define

$$q_{\mathrm{prop}} = \left\lceil \log_2 \frac{T}{NT_{\mathrm{res}}} \right\rceil \tag{14}$$

where $\lceil \cdot \rceil$ is the integer-ceiling operation. If $q > q_{\mathrm{prop}}$, timing synchronization is achieved.

So far, noise has not been considered. The useful waveform may be distorted when noise is taken into account. Thus, a good noise reduction approach should be exploited to obtain more accurate estimation through the above algorithm. Since noise can be approximately treated as a Gaussian random process, a simple and effective noise reduction method is the averaging method. In doing so, the data stream of a training sequence, whose pattern in the system is designed as "$1,-1,1,-1,\ldots$" (actually, the pattern can also be generated randomly), should be transmitted with a sequence length of M bits. Thus, there are M consecutive symbols that could be applied to generate $S_i^{(0)}$ or $S_j^{(q)}$. By averaging the M correlation outcomes, (5) and (8) can be replaced by the following equations:

$$S_i^{(0)} = \frac{1}{M} \left| \sum_{k=0}^{M-1} \int_{\hat{\tau}+iT/N}^{\hat{\tau}+iT/N+T_I} r(t+kT) \times r^*(t+kT+T/2)dt \right|, \qquad i=0,1,\ldots N-1 \tag{15}$$

$$S_j^{(q)} = \frac{1}{M} \left| \sum_{k=0}^{M-1} \int_{\hat{\tau}-(-1)^j \frac{T}{2^qN}}^{\hat{\tau}-(-1)^j \frac{T}{2^qN}+T_I} r(t+kT) \times r^*(t+kT+T/2)dt \right|, \qquad j=0,1. \tag{16}$$

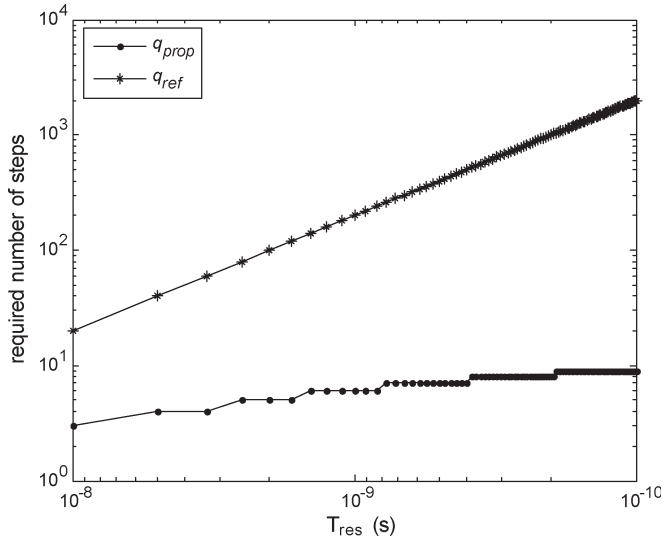

Fig. 3. Required number of steps versus $T_{\rm res}$ ($T = 200$ ns, $N = 4$).

B. Comparison Between the Proposed Algorithm and the Conventional Algorithm

According to the algorithm in [19], the required number of steps for fine timing synchronization is calculated by

$$q_{\rm ref} = \lceil T/(N_f T_{\rm res}) \rceil . \tag{17}$$

Here, N_f is the number of frames per symbol, and $N_f = 1$ as in [19]. By comparing (14) with (17), it is clear that the time complexity of the algorithm in [19] is $O(1/T_{\rm res})$, whereas the counterpart in the new algorithm here is only $O(\log_2(1/T_{\rm res}))$. Fig. 3 shows the required number of steps versus $T_{\rm res}$ when $T = 200$ ns and $N = 4$. One can see that as the synchronization resolution improves, the difference between $q_{\rm ref}$ and $q_{\rm prop}$ becomes bigger. On the other hand, regarding the computational load in data processing, for the proposed algorithm, in step 0, it has $N + 1$ summation and two multiplication operations in view of (6) and (7) (consider T/N as one parameter when T and N are fixed), and in step q ($q \geq 1$), it has two summation and q multiplication operations according to (10) and (11). Thus, the proposed algorithm has a total computational load of $N + 1 + 2q_{\rm prop}$ summation and $2 + \sum_{q=1}^{q_{\rm prop}} q$ multiplication operations. Meanwhile, for the algorithm in [19], which has coarse timing and fine timing, it requires a computational load of about $2 + 2.5q_{\rm ref}$ summation and nine multiplication operations. Notice that for the 64-bit binary double precision floating-point arithmetic specified in the IEEE Standard 754, one multiplication operation is equivalent to at most 63 summation operations. By using $T_{\rm res} = 1/3.952$ ns and $T = 1000$ ns as in [19] for the computational complexity comparison between the two algorithms with $N = 4$, it can be verified that the proposed algorithm has a total computational load of 25 summation and 57 multiplication operations or equivalently 3616 summation operations, whereas the algorithm in [19] has a total computational load of about 9882 summation and 9 multiplication operations or equivalently 10 449 summation operations. It is clear that the new timing synchronization algorithm remarkably shortens the acquisition time and decreases the computational load.

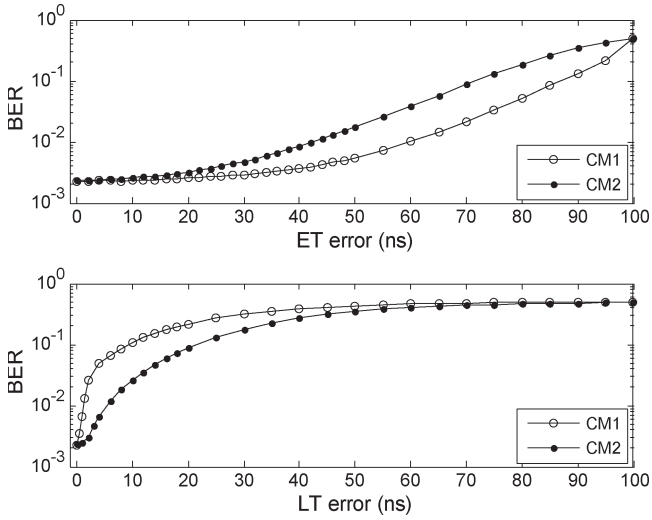

Fig. 4. Effect of timing error on BER performance. The integral interval for demodulation equals $T/2$. The top plot is for ET error; the bottom one is for LT error. The BER of perfect timing (with zero timing error) is also shown for comparison.

IV. Simulation Results

In the simulated system, the parameters are set as follows: symbol period $T = 200$ ns, chaotic pulsewidth $T_w = 2$ ns, sampling frequency for the simulation $f_s = 8$ GHz, and synchronization resolution $T_{\rm res} = 1/f_s$. Moreover, the integral window length in the data demodulation stage is $T/2$, the UWB channels are 802.15.4a CM1 and CM2 channel models [21], i.e., in the residential line-of-sight (LOS) environment and the residential non-LOS (NLOS) environment, respectively. Finally, the chaotic map used for generating chaos is the logistic map [8].

The existence of timing error may induce BER performance degradation. There are three kinds of timing results in general. In this paper, the situations of $\hat{\tau} < \tau - T_{\rm res}$, $\hat{\tau} > \tau + T_{\rm res}$, and $\hat{\tau} \in [\tau - T_{\rm res}, \tau + T_{\rm res}]$ are called earlier timing (ET), later timing (LT), and accurate timing (AT), respectively.

First, the effect of timing error on the BER performance was investigated. Fig. 4 shows BER versus timing error given by $|\hat{\tau} - \tau|$ in CM1 and CM2 at E_b/N_0 of 18 dB, where E_b denotes the signal energy per bit. Considering the BER of perfect timing (with zero timing error) as the benchmark, it can be observed in Fig. 4 that even when the ET error is relatively large (up to about 30 ns in CM1 or about 16 ns in CM2), the BER performance degradation is still slight. On the other hand, even a tiny LT error will induce remarkable performance degradation. It reveals that the presented system performance is highly sensitive to the LT error but insensitive to the ET error. This can be explained as follows. The multipath channel energy mainly falls in the front part of $h(t)$, whereas the rear part contains relatively low and scattered signal energy [21]. Thus, when slight LT occurs, not only is the undesirable interference from the next symbol induced, but also the useful symbol energy collected becomes small, which seriously deteriorates the BER performance.

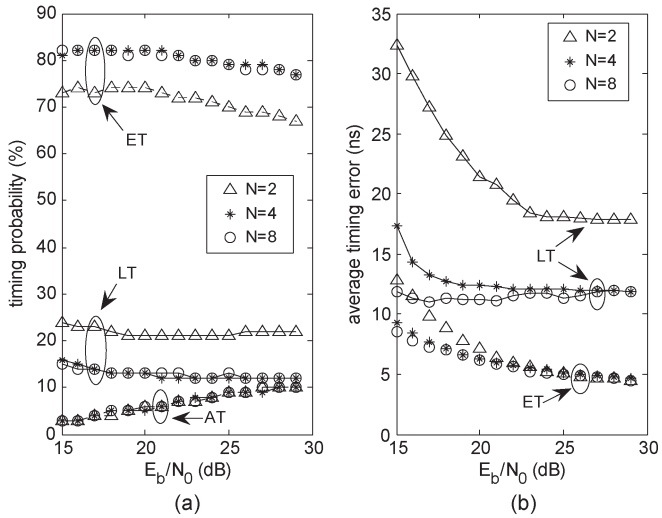

Fig. 5. Comparison among (a) probabilities and (b) average timing errors versus E_b/N_0 under different values of N over CM1.

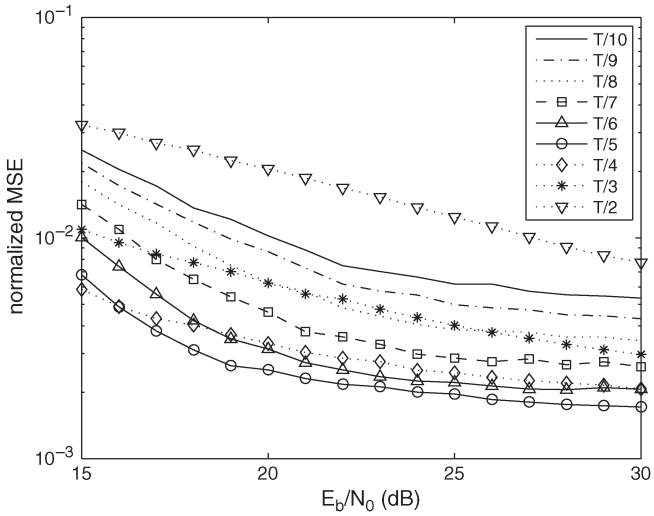

Fig. 6. Normalized MSE versus E_b/N_0 with different integral window lengths (CM1, $M = 8$).

On the other hand, when ET takes place with a relatively large error, the loss of current symbol energy and the interference from the previous symbol are both relatively small, and therefore, the performance degradation is not significant. Noticing that the channel multipath delay spread of CM1 (LOS) is smaller than that of CM2 (NLOS) [21], the rear part of $h(t)$ contains less multipath energy in CM1 than in CM2. This implies that the system is more insensitive to the ET error in CM1 than in CM2. Meanwhile, CM1 has a power delay profile (PDP) in a decreasing shape, whereas CM2 exhibits a first-increasing-and-then-decreasing PDP shape [21], and hence, the beginning part of $h(t)$ contains more multipath energy in CM1 than in CM2. This shows that the system is more sensitive to the LT error in CM1 than in CM2.

Furthermore, it was tested as how different values of N affect the timing synchronization performance. Fig. 5 shows the occurrence probabilities of ET, LT, and AT and the average timing errors of ET and LT statistically in the cases of $N = 2$, $N = 4$, and $N = 8$ in CM1 all through 10 000 simulation runs. Since the BER performance is highly sensitive to LT but less sensitive to ET, it is clear that the larger the probability of LT is, the worse the BER performance will be, and the smaller the average timing error is, the better the BER performance becomes. Accordingly, one can find in Fig. 5 that the two cases of $N = 4$ and $N = 8$ have similar probability performance, yet, the case of $N = 8$ has slightly better timing error performance than the case of $N = 4$. The two cases both have better probability and timing error performance than the case of $N = 2$. On the other hand, for larger N, more integral operations need to be performed during every symbol observation interval, which requires more implementation complexity. Hence, $N = 4$ was chosen in the subsequent simulation for a performance–complexity tradeoff.

As mentioned in Section III-A, different integral window lengths in the synchronizing stage yield different synchronization accuracy degrees, as visualized in Fig. 6, which shows the normalized mean square error (MSE) given by $E\{(\hat{\tau} - \tau)^2\}/T^2$ versus E_b/N_0 in CM1 with the training sequence length $M = 8$, where $E\{\cdot\}$ denotes the expectation operation. It can be observed that $T_I = T/5$ results in the smallest normalized MSE as compared to the others, i.e., $\{T/2, T/3, T/4, T/6, T/7, T/8, T/9, T/10\}$ in CM1, when $E_b/N_0 \geq 16$ dB. Consequently, T_I is set as T/5 for the CM1 channel. Thus, the best one was chosen through simulation as integral window length, i.e., $T/3$, in the synchronization stage for the CM2 channel. Some other figures with the CM2 channel and different training sequence lengths are not shown here for brevity. Notice that there exists an optimal T_I, which can be explained as follows. In the synchronizing stage, the integral window length will determine the amount of collected useful signal energy, interference signal energy (from neighboring symbols), and noise energy. If the integral window is very long, the increment of the interference energy and noise energy collected may become larger than the increment of the useful signal energy collected; on the other hand, if the integral window is very short, the useful signal energy collected may become very small. Furthermore, it is found that the optimal T_I is related to the channel model, because different channel models exhibit different impulse response durations and the optimal T_I increases with the impulse response duration.

Based on the above setup, 10 000 runs were performed for the timing synchronization test. Figs. 7 and 8 show the timing results in CM1 and CM2, respectively. The left and right subfigures of each figure represent timing occurrence probability versus E_b/N_0 and average timing error versus E_b/N_0, with $M = \{1, 2, 4, 8, 16\}$, respectively. It can be seen that in CM1, the probability of LT decreases and the probability of AT increases as E_b/N_0 increases. Moreover, ET occupies a large proportion of probability, whereas LT occurs in relatively small probability. Meanwhile, the average timing errors of ET and LT both decrease monotonically as E_b/N_0 increases, and the timing performance is improved monotonically as M increases. The average timing errors of ET and LT are less than 13 and 7 ns, respectively, when $E_b/N_0 \geq 19$ dB and $M \geq 8$ in CM1. Concerning CM2, it can be observed that when

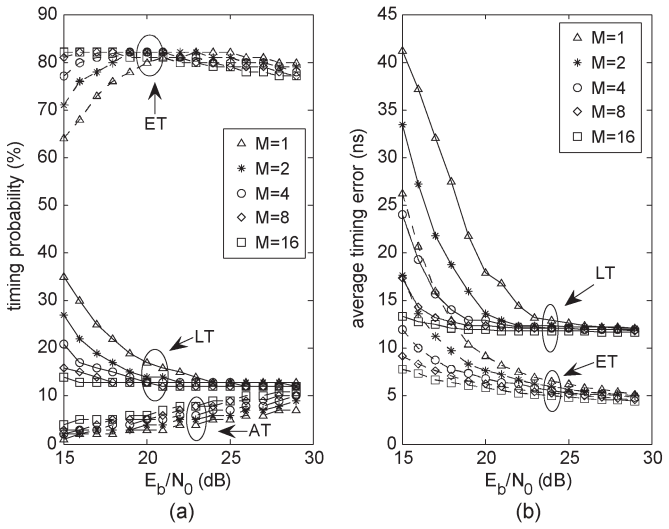

Fig. 7. (a) Timing probability and (b) average timing error versus E_b/N_0, with $M = \{1, 2, 4, 8, 16\}$ (CM1).

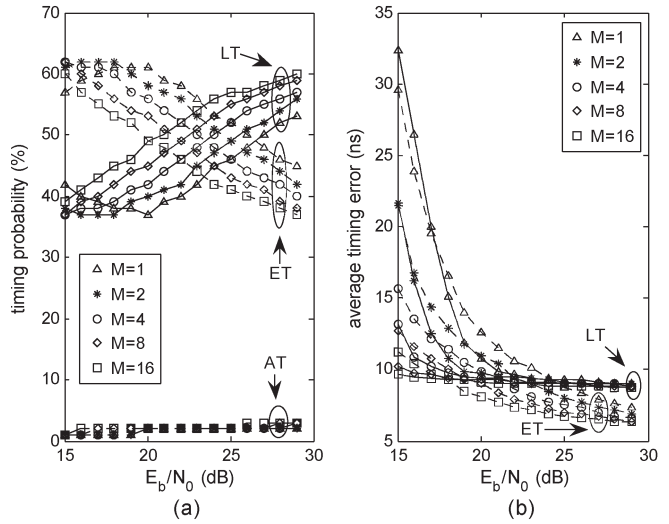

Fig. 8. (a) Timing probability and (b) average timing error versus E_b/N_0, with $M = \{1, 2, 4, 8, 16\}$ (CM2).

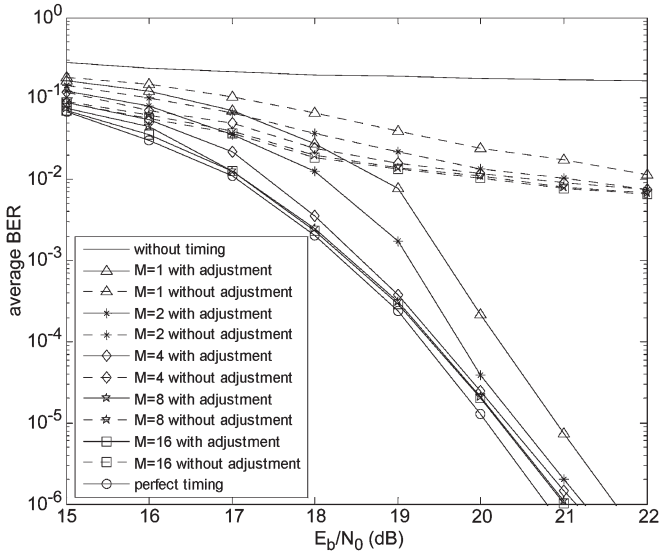

Fig. 9. Average BER versus E_b/N_0, with $M = \{1, 2, 4, 8, 16\}$ (CM1).

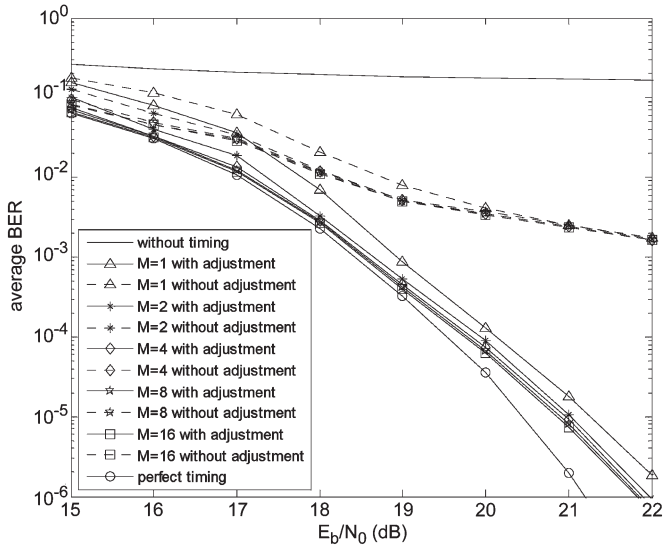

Fig. 10. Average BER versus E_b/N_0, with $M = \{1, 2, 4, 8, 16\}$ (CM2).

$E_b/N_0 \geq 20$ dB, the probability of LT increases as E_b/N_0 increases, whereas the probability of ET decreases as E_b/N_0 increases, and these two quantities are comparable, which is somewhat different from CM1. The average timing error in CM2 has the same trend as that in CM1.

Returning to Fig. 4, one can see that the presented system can tolerate a relatively large ET error. However, even a tiny LT error is not welcome. Additionally, it can be observed from Figs. 7 and 8 that not only does the summation of the average ET error and the average LT error become smaller as M and E_b/N_0 increase, but also when $E_b/N_0 > 20$ dB and $M = 16$, this summation is less than the acceptable ET error (about 30 ns) in CM1 and is almost the same as that (about 16 ns) in CM2. Consequently, in order to minimize the probability of LT to the utmost extent, the estimated integral starting point $\hat{\tau}$ is adjusted ahead by λ, i.e., the final integral starting point estimated is $\hat{\tau} - \lambda$ (timing with this operation is called timing with adjustment, and timing without this operation is called timing without adjustment below). In the simulation, the average LT error at the E_b/N_0 of 21 dB was taken as λ for CM1, and the average LT error at the E_b/N_0 of 22 dB was regarded as λ for CM2.

Finally, the BER performances of timing with adjustment, timing without adjustment, without timing, and perfect timing are all compared. Figs. 9 and 10 show the average BER versus E_b/N_0 in CM1 and CM2, respectively. One can observe that when the training sequence length $M \geq 2$, the BER performance of the system is improved, as compared to that with $M = 1$, thanks to the averaging operation for the noise reduction. Moreover, the BER decreases monotonically as M increases. Meanwhile, it can be observed that timing with adjustment offers a significantly improved BER performance as compared to that without adjustment, and the BER performances of timing with adjustment are only about 0.2 dB and about 0.6 dB worse than those of perfect timing at the BER of 10^{-6} when $M = 16$ in CM1 and CM2, respectively.

V. Conclusion

Timing synchronization is a critical issue in UWB radios. In this paper, a fast and low-complexity timing synchronization algorithm depending on training sequences has been developed and tested for the FM-DCSK UWB system, which is attributed to the outstanding correlation characteristic of chaotic signals. Simulation results have shown that the performance of FM-DCSK UWB based on the new algorithm is very close to that with perfect timing. Timing adjustment operation is necessary and helpful. Compared to the linear and approximately exhaustive searching scheme [19], the new timing algorithm shortens the searching interval by at least a half in size at every step, therefore significantly improving the acquisition speed and remarkably decreasing the computational complexity. It is believed that the new timing algorithm is particularly suitable for FM-DCSK UWB and DCSK [22] UWB [23] systems, which are considered as good candidates for low-rate WPAN applications with low power and low complexity.

In the next phase of this work, the possibility of developing a novel timing tracking algorithm with phase-locked loop [24]–[27] will be explored.

Acknowledgment

The authors would like to thank W. Xu, X. Min, D. Xie, and Z. Xu for their valuable suggestions and helpful discussions.

References

[1] V. C. Gungor and G. P. Hancke, "Industrial wireless sensor networks: Challenges, design principles, and technical approaches," *IEEE Trans. Ind. Electron.*, vol. 56, no. 10, pp. 4258–4265, Oct. 2009.

[2] X. Chen and S. Kiaei, "Monocycle shapes for ultra wideband system," in *Proc. Int. Conf. Circuits Syst.*, Scottsdale, AZ, May 25–29, 2002, pp. 597–600.

[3] C. Carbonelli and U. Mengali, "Synchronization algorithms for UWB signals," *IEEE Trans. Commun.*, vol. 54, no. 2, pp. 329–338, Feb. 2006.

[4] C. Carbonelli, S. Vedantam, and U. Mitra, "Sparse channel estimation with zero tap detection," *IEEE Trans. Wireless Commun.*, vol. 6, no. 5, pp. 1743–1753, May 2007.

[5] R. Hoctor and H. Tomlinson, "Delay-hopped transmitted-reference RF communications," in *Proc. IEEE Conf. Ultra-Wideband Syst. Technol.*, Baltimore, MD, May 21–23, 2002, pp. 265–269.

[6] G. Kolumban, M. P. Kennedy, G. Kis, and Z. Jako, "FM-DCSK: A novel method for chaotic communications," in *Proc. IEEE Int. Symp. Circuits Syst.*, 1998, pp. 477–480.

[7] G. Kolumban, "UWB technology: Chaotic communications versus noncoherent impulse radio," in *Proc. Eur. Conf. Circuit Theory Des.*, 2005, pp. 79–82.

[8] C. K. Tse and F. C. M. Lau, *Chaos-Based Digital Communication Systems*. New York: Springer-Verlag, 2003.

[9] G. Kolumban, M. P. Kennedy, and L. O. Chua, "The role of synchronization in digital communications using chaos—Part 1: Fundamentals of digital communications," *IEEE Trans. Circuits Syst. I, Fundam. Theory Appl.*, vol. 44, no. 10, pp. 927–936, Oct. 1997.

[10] M. P. Kennedy, G. Kolumban, G. Kis, and Z. Jako, "Performance evaluation of FM-DCSK modulation in multipath environments," *IEEE Trans. Circuits Syst. I, Fundam. Theory Appl.*, vol. 47, no. 12, pp. 1702–1711, Dec. 2000.

[11] L. Ye, G. Chen, and L. Wang, "Essence and advantages of FM-DCSK technique versus conventional spread-spectrum communication methods," *Circuits Syst. Signal Process.*, vol. 24, no. 5, pp. 657–673, Sep./Oct. 2005.

[12] L. Wang, C. Zhang, and G. Chen, "Performance of an SIMO FM-DCSK communication system," *IEEE Trans. Circuits Syst. II, Exp. Briefs*, vol. 55, no. 5, pp. 457–461, May 2008.

[13] X. Min, W. Xu, L. Wang, and G. Chen, "Promising performance of a frequency-modulated differential chaos shift keying ultra-wideband system under indoor environments," *IET Commun.*, vol. 4, no. 2, pp. 125–134, Jan. 2010.

[14] Z. Tian and G. B. Giannakis, "BER sensitivity to mistiming in ultra-wideband impulse radios—Part 1: Nonrandom channels," *IEEE Trans. Signal Process.*, vol. 53, no. 4, pp. 1550–1560, Apr. 2005.

[15] N. He and C. Tepedelenlioglu, "Performance analysis of non-coherent UWB receivers at different synchronization levels," *IEEE Trans. Wireless Commun.*, vol. 5, no. 6, pp. 1266–1273, Jun. 2006.

[16] E. A. Homier and R. A. Scholtz, "Rapid acquisition of ultra-wideband signals in the dense multipath channel," in *Proc. IEEE Conf. Ultra Wideband Syst. Technol.*, 2002, pp. 105–109.

[17] L. Wu, V. Lottici, and Z. Tian, "Maximum likelihood multiple access timing synchronization for UWB communications," *IEEE Trans. Wireless Commun.*, vol. 7, no. 11, pp. 4497–4501, Nov. 2008.

[18] Z. Tian and G. B. Giannakis, "A GLRT approach to data-aided timing acquisition in UWB radios—Part 1: Algorithms," *IEEE Trans. Wireless Commun.*, vol. 4, no. 6, pp. 2956–2967, Nov. 2005.

[19] R. Zhang and X. Dong, "Synchronization and integration region optimization for UWB signals with non-coherent detection and auto-correlation detection," *IEEE Trans. Commun.*, vol. 56, no. 5, pp. 790–798, May 2008.

[20] L. Yang and G. Giannakis, "Timing ultra-wideband signals with dirty templates," *IEEE Trans. Commun.*, vol. 53, no. 11, pp. 1952–1963, Nov. 2005.

[21] A. F. Molisch, K. Balakrishnan, C.-C. Chong, S. Emami, A. Fort, J. Karedal, J. Kunisch, H. Schantz, U. Schuster, and K. Siwiak, IEEE 802.15.4a channel model—Final report, Tech. Rep. Document IEEE 802.15-04-0662-02-004a. [Online]. Available: http://www.ieee802.org/15/pub/2004/

[22] G. Kolumban, B. Vizvari, W. Schwarz, and G. Abel, "Differential chaos shift keying: A robust coding for chaos communication," in *Proc. Int. Workshop Non-linear Dyn. Electron. Syst.*, Seville, Spain, Jun. 1996, pp. 87–92.

[23] C. C. Chong and S. K. Yong, "UWB direct chaotic communication technology for low-rate WPAN applications," *IEEE Trans. Veh. Technol.*, vol. 57, no. 3, pp. 1527–1536, May 2008.

[24] G. Fedele, C. Picardi, and D. Sgro, "A power electrical signal tracking strategy based on the modulating functions method," *IEEE Trans. Ind. Electron.*, vol. 56, no. 10, pp. 4079–4087, Oct. 2009.

[25] M. A. Perez, J. R. Espinoza, L. A. Moran, M. A. Torres, and E. A. Araya, "A robust phase-locked loop algorithm to synchronize static-power converters with polluted AC systems," *IEEE Trans. Ind. Electron.*, vol. 55, no. 5, pp. 2185–2192, May 2008.

[26] Y. W. Li, B. Wu, D. Xu, and N. R. Zargari, "Space vector sequence investigation and synchronization methods for active front-end rectifiers in high-power current-source drives," *IEEE Trans. Ind. Electron.*, vol. 55, no. 3, pp. 1022–1034, Mar. 2008.

[27] R. M. Santos Filho, P. F. Seixas, P. C. Cortizo, L. A. B. Torres, and A. F. Souza, "Comparison of three single-phase PLL algorithms for UPS applications," *IEEE Trans. Ind. Electron.*, vol. 55, no. 8, pp. 2923–2932, Aug. 2008.

Shaoyuan Chen (S'10) received the B.S. degree in communication engineering from Xiamen University, Fujian, China, in 2007, where he is currently working toward the Ph.D. degree in the Department of Communication Engineering.

His research interests include synchronization, channel estimation, and transceiver design and optimization of ultrawideband and chaotic communications.

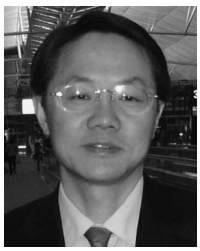

Lin Wang (S'99–M'03–SM'09) received the B.Sc. degree in mathematics (with first-class honors) from Chongqing Normal University, Chongqing, China, in 1984, the M.Sc. degree in applied mathematics from Kunming University of Technology, Kunming, China, in 1988, and the Ph.D. degree in electronics engineering from the University of Electronic Science and Technology of China, Chengdu, China, in 2001.

From 1984 to 1986, he was a Teaching Assistant in the Department of Mathematics, Chongqing Normal University. From 1989 to 2002, he was a Teaching Assistant, a Lecturer, and then an Associate Professor in applied mathematics and communication engineering at the Chongqing University of Post and Telecommunication. From 1995 to 1996, he spent one year in the Department of Mathematics, University of New England, Armidale, Australia. In 2003, he spent three months as a Visiting Researcher at the Center for Chaos and Complexity Networks, City University of Hong Kong, Hong Kong. Since 2002, he has been a Full Professor and an Associate Dean of the School of Information Science and Technology, Xiamen University, Xiamen, China. He is the author of over 60 published journal and conference papers. He is the holder of five patents in the field of physical-layer digital communications. His current research interests include channel coding and chaos modulation and their applications to wireless communications and storage systems.

Guanrong (Ron) Chen (M'89–SM'92–F'97) received the M.Sc. degree in computer science from Sun Yat-Sen (Zhongshan) University, Guangzhou, China, in 1981, and the Ph.D. degree in applied mathematics from Texas A&M University, College Station, in 1987.

He is currently Chair Professor and the Director of the Centre for Chaos and Complex Networks, City University of Hong Kong, Hong Kong. He is an Honorary Professor at different ranks in more than 30 universities worldwide.

Dr. Chen serves as an Editor for several IEEE TRANSACTIONS and international journals. He is a highly cited researcher in engineering according to Thomson Reuters, received four best SCI journal paper awards in 1998, 2001, 2002, and 2005, and the 2008 State Natural Science Award of China.